Self-organization of channels and hillslopes in models of fluvial landform evolution

Stefan Hergarten[1] and Alexa Pietrek[1]

[1]Institut für Geo- und Umweltnaturwissenschaften, Albert-Ludwigs-Universität Freiburg, Albertstr. 23B, 79104 Freiburg, Germany

Correspondence: Stefan Hergarten
(stefan.hergarten@geologie.uni-freiburg.de)

Abstract. Including hillslope processes in models of fluvial landform evolution is still challenging. Since applying the respective models for fluvial and hillslope processes to the entire domain causes scaling problems and makes the results dependent on the spatial resolution, the domain is explicitly subdivided into channels and hillslopes in some models. The transition from hillslopes to channels is typically attributed to a given threshold catchment size as a proxy for a minimum required discharge. Here we propose a complementary approach for delineating channels based on the discrete representation of the topography. We assume that sites with only one lower neighbor are channelized. In combination with a suitable model for hillslope processes, this concept initiates a self-organization of channels and hillslopes. A numerical analysis with a simple model for hillslope dynamics reveals no scaling issues, so that the results appear to be independent of the spatial resolution. The approach predicts a break in slope in the sense that all channels are distinctly less steep than hillslopes. On a regular lattice, the simple D8 flow routing scheme (steepest descent among the 8 nearest and diagonal neighbors) harmonizes well with the concept proposed here. The D8 scheme works well even when applied to the hillslopes. This property simplifies the numerical implementation and increases its efficiency.

1 Introduction

Models of the stream-power type have been successfully applied in modeling fluvial landform evolution at large scales for a long time (for an overview, see, e.g., Coulthard, 2001; Willgoose, 2005; Wobus et al., 2006; van der Beek, 2013). Instead of simulating the processes in a river in detail, these models describe the long-term contribution of river segments to landform evolution based on strongly simplified relations. The stream-power incision model (SPIM) is the simplest model of this type. It predicts the erosion rate E as a function of the upstream catchment size A (a proxy for the mean discharge) and the channel slope S in the form

$$E = KA^m S^n. \tag{1}$$

The SPIM involves only three parameters, K, m, and n. The ratio of the exponents m and n is constrained quite well by long profiles of real-world rivers. Hack (1957) found the relation

$$S \propto A^{-\theta}, \tag{2}$$

25 $\theta = 0.45$ or $\theta = 0.5$ is typically used as a reference value (e.g., Whipple et al., 2013; Lague, 2014). Interpreting Eq. (2) as
the fingerprint of spatially uniform erosion yields $\frac{m}{n} = \theta$. The absolute values of m and n are, however, more uncertain (e.g.,
Lague, 2014; Harel et al., 2016; Hilley et al., 2019; Adams et al., 2020). The widely used choice $n = 1$ is mainly a matter of
convenience since the model is linear with regard to the channel slope S (and this also with regard to the surface elevation) then.
The third parameter, K, is called the erodibility. It is a lumped parameter that summarizes all influences on erosion beyond

30 catchment size and channel slope.

The SPIM implements the concept of detachment-limited erosion (Howard, 1994) in the sense that all particles entrained by
the river are immediately swept out of the system. This means that the effect of sediment transport on landform evolution is
completely disregarded, which is obviously a severe limitation.

Furthermore, the SPIM is in principle a one-dimensional model. Its simplest implementation in a two-dimensional landform

35 evolution model assumes that each node is connected to some of its neighbors by channels. Since the minimum catchment
size is defined by one grid cell, an increase in spatial resolution causes an increase in maximum equilibrium channel slopes
according to Eq. (2). This leads to canyon-type topographies with properties depending on the spatial resolution. In order to
avoid the occurrence of such unrealistic topographies, models of fluvial landform evolution need to be extended by hillslope
processes, where the linear diffusion equation is the simplest model.

40 However, simply adding a diffusion term (or any more elaborate model for hillslope processes) to the SPIM causes a scaling
problem, owing to the transport of material from the hillslopes into the rivers. Even the properties of large rivers become
strongly dependent on the spatial resolution then. In order to overcome this problem, subpixel representations of the rivers
where a river segment only covers a fraction of a grid cell were proposed (Howard, 1994; Perron et al., 2008; Pelletier, 2010).
However, these approaches are also not free of problems as discussed by Hergarten (2020a).

45 Discriminating rivers by a threshold catchment size A_{c} and separating the domain accordingly into hillslope ($A < A_{\mathrm{c}}$) and
channel sites ($A \geq A_{\mathrm{c}}$) is an alternative concept for avoiding the scaling problem. In the simplest version of this concept (e.g.,
Campforts et al., 2017), sediment fluxes from hillslopes into rivers are disregarded, reflecting the idea that all hillslope material
entering the rivers is immediately swept out of the system without any effect on the rivers. However, the interaction between
rivers and hillslopes is unidirectional then without any feedback of the hillslopes on the rivers and thus on large-scale landform

50 evolution. The approach proposed by Hergarten (2020a) overcomes this limitation, but requires a rescaling of the erodibility
K with the threshold catchment size A_{c}. While this approach has some advantages over the earlier approaches, the question
remains whether it makes sense to squeeze the sediment flux from the hillslopes into the framework of detachment-limited
erosion.

Furthermore, separating rivers from hillslopes at a given threshold catchment size requires an adjustment of the parameters of

55 the erosion models used for the two domains in order to avoid weird topographies at the transition. As an additional challenge,
the distinction by a given threshold catchment size A_{c} may also generate an artificial dependence on the spatial resolution.
While catchment size is useful in the context of the SPIM for channelized flow, it is not necessarily well-defined on hillslopes.
In the extreme scenario of parallel flow on a planar hillslope, A is proportional to the grid spacing. So the point where $A \geq A_{\mathrm{c}}$

on a hillslope depends on the grid spacing. Catchment size per unit width would be the right property here (Bonetti et al., 2018), but this property is not compatible with the SPIM in its simplest form.

While extensions of the SPIM towards sediment transport have been available for several years (Whipple and Tucker, 2002; Davy and Lague, 2009), considerable progress was recently made concerning their numerical treatment (Yuan et al., 2019; Hergarten, 2020b). In particular, the fully implicit scheme for the linear model ($n = 1$) proposed by Hergarten (2020b) achieves almost the same performance as the implicit scheme for the SPIM (Hergarten and Neugebauer, 2001; Braun and Willett, 2013). The numerical progress allows not only for considering larger domains and longer time spans, but also for higher spatial resolutions. In turn, the need to include hillslope processes in a consistent way increases.

In this study, the shared stream-power model

$$\frac{E}{K_\mathrm{d}} + \frac{Q}{K_\mathrm{t}A} = A^m S^n \tag{3}$$

is used, where Q is the sediment flux (volume per time). While the SPIM (Eq. 1) uses a single lumped parameter for the erodibility, the shared stream-power model involves two parameters K_d and K_t with the same physical units. The shared stream-power model is mathematically equivalent to the linear decline model (Whipple and Tucker, 2002) and to the ξ–q model (Davy and Lague, 2009).

While the the equation for the change in surface elevation H at a given uplift rate U is the same as for the SPIM (and other models in this context),

$$\frac{\partial H}{\partial t} = U - E, \tag{4}$$

taking into account sediment transport requires an additional balance equation. Assuming that each node i of a discrete grid delivers its entire sediment flux Q_i to a single neighbor, the sediment balance equation reads

$$E_i = \frac{Q_i - \sum_j Q_j}{s_i}, \tag{5}$$

where s_i is the size (area) of the respective grid cell. The right-hand side of Eq. (5) is a discrete representation of the divergence operator with the sum extending over all neighbors j that deliver their sediment flux to the cell i.

Since the shared stream-power model only serves as an example in this study, only its most important properties are described in the following, and readers are referred to previous work (Hergarten, 2020b, 2021). The parameter K_d describes the ability to erode the bedrock, while the transport capacity

$$Q_\mathrm{c} = K_\mathrm{t} A^{m+1} S^n \tag{6}$$

(the sediment flux at $E = 0$) depends on K_t. The model turns into the SPIM for $K_\mathrm{t} \to \infty$ and into a transport-limited model for $K_\mathrm{d} \to \infty$.

For spatially uniform erosion, the sediment flux is $Q = EA$, and Eq. (3) collapses to a form analogous to the SPIM (Eq. 1) with an effective erodibility K according to

$$\frac{1}{K} = \frac{1}{K_\mathrm{d}} + \frac{1}{K_\mathrm{t}}. \tag{7}$$

90 Therefore, equilibrium topographies under uniform uplift depend only on K, but not on the individual values K_d and K_t. In particular, the channel slope is

$$S = \left(\frac{E}{KA^m} \right)^{\frac{1}{n}}. \tag{8}$$

In the following section, we introduce a simple scheme for delineating channels on a given topography without defining a threshold catchment size explicitly. After finding that this scheme is not applicable to digital terrain models (DTMs) of
95 real-world topographies in its simplest form, it will be shown in Sect. 3 that it works well in combination with self-organized drainage patterns in numerical models.

2 A simple criterion for delineating channels

The simplest scheme of flow routing on a given topography assumes that the discharge of each cell is entirely delivered to one of its neighbors. This neighbor is typically selected by the steepest-descent criterion, so by the maximum ratio of elevation
100 drop and horizontal distance. This ratio also defines the channel slope S. On regular meshes, the D8 flow routing scheme (O'Callaghan and Mark, 1984) taking into account the eight nearest and diagonal neighbors is widely used. In turn, more elaborate flow routing schemes such as the MFD (multiple flow directions) scheme (Freeman, 1991; Quinn et al., 1991) or the D∞ scheme (Tarboton, 1997) are able to distribute the discharge among multiple neighbors.

Instead of introducing a minimum catchment size as a criterion for channelized flow, we simply define sites that have only
105 one neighbor with a lower elevation as channel sites. For such sites, the D8 scheme (or an equivalent single-flow direction scheme on an irregular grid) would capture the flow direction well, and schemes using multiple neighbors would not yield a different result. This concept reflects the idea that a thin layer of water is focused into one direction without spreading laterally.

As a second rule for delineating channels, we assume that the flow target of a channel site is also a channel site even if it has more than one lower neighbor. This means that a channel never turns into distributed flow. While this rule is not relevant for
110 the examples considered in this study, it may become important for rivers in a rather flat, tectonically inactive foreland region (e.g., Hergarten, 2022a).

Figure 1 shows the number of channel heads (the uppermost point of each channel) obtained by applying this concept to three topographies. The first topography is a fluvial equilibrium topography under uniform uplift computed on a 5000×5000 grid for $m = 0.5$ and $n = 1$ in nondimensional coordinates ($K = 1$, $U = 1$). This topography was also used by Hergarten (2020b)
115 and Hergarten (2021) and is shown in Fig. 2.

Formally, only about 25 % of all nodes (6.3 millions out of 25 millions) are channel sites according to the criterion defined above. This result is owing to the large number of small catchments. The flow pattern contains almost 15 million single-pixel catchments, of which only about 5200 are channelized. It is indeed very unlikely that a single-pixel catchment meets our criterion for channels. In this case, 7 out of its 8 neighbors must be higher than the considered sites, but none of them may
120 drain towards this site.
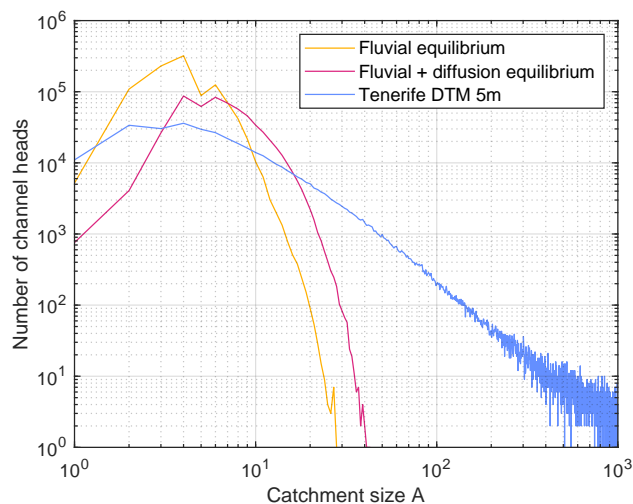
Figure 1. Size distribution of the channel heads detected on two synthetic topographies and a DTM of Tenerife. The numbers refer directly to the catchment size measured in pixels without binning.
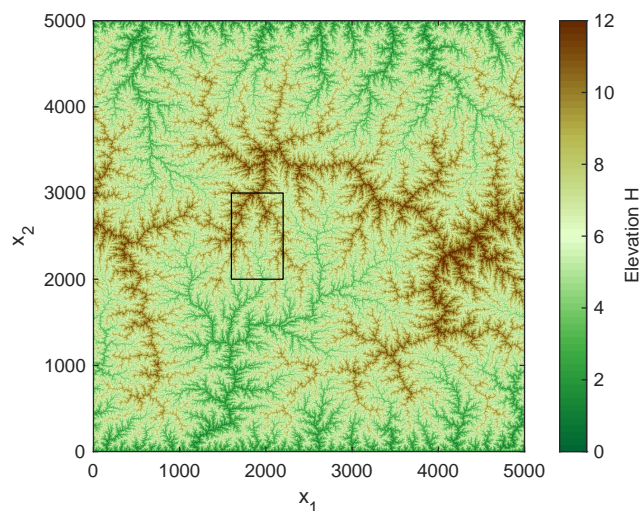
Figure 2. Fluvial equilibrium topography on a 5000×5000 grid obtained by Hergarten (2020b). The rectangle defines the region considered in Fig. 3.

According to Fig. 1, the most frequent catchment size of the channel heads is 4 pixels, and all nodes with catchment sizes $A > 32$ pixels are channelized. So our criterion for channelization does not capture all points of a fully fluvial topography, but the deviations are limited to small catchment sizes.

The second example is basically the same topography, but simulated with transport-limited fluvial erosion and linear diffusion applied to the entire domain. A moderate value of the diffusivity, $D = 1$, was chosen since switching from the SPIM to the

125

transport-limited model solves some of the scaling issues discussed in Sect. 1, but still generates artifacts if diffusion becomes strong. The effect of diffusion on the topography would hardly be visible at the scale of Fig. 2 for $D = 1$. Nevertheless, the distribution of the channel heads has shifted by a factor of about 1.5 to 2 in catchment size. So the smoothing of the topography is in principle detected by the simple scheme for delineating channels.

130   As a third example, the 5 m DTM of the Tenerife island (CNIG, 2022) is considered. The limited applicability of our definition to real-world topographies becomes visible here. There are indeed channel heads with a catchment size of several hundred pixels, and the mean catchment size of all channel heads, about 34 pixels, is considerably larger than for the synthetic fluvial topography. However, this mean catchment size is less than 1000 m^2 and thus clearly too small for the occurrence of permanent channels. The most frequent channel-head size is even the same as for the artificial fluvial topography (4 pixels or

135   100 m^2) and thus much to small for real channels.

These results suggest that the simple scheme for delineating channels without an additional threshold is unsuitable for application to real-world terrain models, while it may be useful in the context of modeled topographies.

3   Self-organization of drainage networks

Let us briefly recall some elements of the theory of minimum energy dissipation in river networks introduced in the 1990s

140   (Howard, 1990; Rodriguez-Iturbe et al., 1992a, b; Rinaldo et al., 1992, 1998), leading to the concept of optimal channel networks (OCNs). If we neglect changes in kinetic energy, a channel segment with a length l, a channel slope S, and a discharge q (volume per time) dissipates a power

$$P = \rho g q l S, \tag{9}$$

where ρg is the specific weight of water. Since the mean discharge is proportional to the catchment size under uniform precip-

145   itation, the mean dissipation is

$$\overline{P} \propto AS, \tag{10}$$

and in combination with Hack's relation (Eq. 2)

$$\overline{P} \propto A^{1-\theta}. \tag{11}$$

So the increase in dissipated power with catchment size is weaker than linear as long as $\theta > 0$. Then a single channel with a

150   catchment size A is energetically favorable over two channels with $\frac{A}{2}$ each. This is the main reason why the concept of OCNs predicts dendritic networks instead of parallel channels.

Although there is no rigorous proof of the relevance of minimum energy dissipation for real landform evolution, this result provides an idea how to construct a model with self-organizing channels and hillslopes. The fluvial erosion model in its original form, e.g., the SPIM (Eq. 1) or the shared stream-power model (Eq. 3) should only be applied to channelized sites according

155   to the criterion defined in Sect. 2. In turn, we need a model for hillslopes that does not favor dendritic networks energetically.

Then there is a chance that parts of the domain do not self-organize towards dendritic channel networks. Otherwise, we should expect that the entire area will be captured by channel networks, and that hillslopes will be limited to sites with catchment sizes of only a few pixels, as found for the entirely fluvial topography in Sect. 2.

Any version of the shared-stream power model (Eq. 3) with $m \leq 0$ and $n > 0$ satisfies the condition that dendritic networks
160 are not energetically favored since $\theta = \frac{m}{n} \leq 0$ in equilibrium. While $m < 0$ results in convex equilibrium profiles, $m = 0$ generates straight slopes. The shared stream-power model with $m = 0$ can be interpreted in the way that the ability to erode is independent of the discharge and that the transport capacity (Eq. 6) is proportional to the discharge.

The choice $m = 0$ is appealing since it circumvents the problem that the catchment size A (or the discharge) is not suitable for describing unchannelized flow. For $m < 0$, we would need a model written in terms of catchment size per unit width or
165 discharge per unit width. In turn, the term $\frac{Q}{A}$ at the left-hand side of Eq. (3) does not cause any problem because considering both the sediment flux Q and the catchment size A per unit width would not change their ratio.

The respective detachment-limited version with $m = 0$ and $n = 1$ was already proposed by Carretier et al. (2016), who assumed that the erosion rate at hillslopes is proportional to the slope without any dependence on catchment size. Carretier et al. (2016) compared this model to the nonlinear diffusion model introduced by Roering et al. (1999), which is nowadays
170 widely used, but numerically challenging (Perron, 2011). While it was found that the parameter values can be calibrated to obtain a similar behavior with straight slopes, we should be aware that the ideas behind both models differ fundamentally. The nonlinear diffusion model imposes an absolute upper limit for the slope, while the equilibrium slope still depends on the uplift rate for the shared stream-power model with $m = 0$.

4 A numerical test

175 In this section, we test the criterion for delineating channels proposed in Sect. 2 in combination with the linear version of the shared stream-power model ($n = 1$). Let us assume that hillslopes are also described by the shared stream-power law (Eq. 3) with $m = 0$ and erodibilities $\tilde{K}_\mathrm{d}$ and $\tilde{K}_\mathrm{t}$. For simplicity, we assume

$$\frac{\tilde{K}_\mathrm{d}}{K_\mathrm{d}} = \frac{\tilde{K}_\mathrm{t}}{K_\mathrm{t}} \tag{12}$$

and define

180 $$A_\mathrm{h} = \left(\frac{\tilde{K}_\mathrm{d}}{K_\mathrm{d}}\right)^{\frac{1}{m}} = \left(\frac{\tilde{K}_\mathrm{t}}{K_\mathrm{t}}\right)^{\frac{1}{m}}. \tag{13}$$

Then the hillslopes are described by the same equation as the rivers (Eq. 3) even with the same values of m, K_d, and K_t, but with A_h instead of A at the right-hand side. Accordingly, A_h defines the catchment size above which the erosion by channelized flow is stronger than erosion at hillslopes at the same channel slope S. Using A_h instead of $\tilde{K}_\mathrm{d}$ and $\tilde{K}_\mathrm{t}$ will facilitate the interpretation of the results.

185 The results shown in the following were obtained with the parameter combination $K_\mathrm{d} = K_\mathrm{t} = 2$, which can be seen as the middle between the detachment-limited model and the transport-limited model with an effective erodibility $K = 1$ (Eq. 7).

However, additional simulations with the detachment-limited model and the transport-limited model revealed that none of the results rely on this choice.

Since the catchment size has no effect on erosion for $m = 0$, the choice of the flow routing scheme for hillslopes is not
190 crucial. However, it is important that the same scheme is applied to sediment fluxes and catchment sizes in order to keep the ratio $\frac{Q}{A}$ occurring in Eq. (3) consistent. Adopting the D8 scheme from the channelized sites simplifies the implementation and has the advantage that the fully implicit scheme proposed by Hergarten (2020b) can be used. So we apply the D8 scheme to all sites. Although it is in general not well-suited for hillslopes, we will see in Sect. 6 that it works quite well for the model considered here.

195 Simulations were performed for $A_\mathrm{h} = 10$, 100, and 1000, starting from the fluvial equilibrium topography shown in Fig. 2. The simulations were run with a time increment $\delta t = 10^{-3}$. A steady state in the strict sense was not achieved in any of the simulations. A considerable number of changes in flow direction (at about 2 % of all grid cells) occurs in each time step. However, these changes mainly affect the hillslopes, while changes in channels and transitions between channels and hillslopes are rare. The results presented in the following were derived from the topography at a large time $t = 100$ in order to ensure that
200 there is no systematic change in topography anymore.

Figure 3 shows the parts of the obtained topography defined by the rectangle in Fig. 2. It is immediately recognized that the canyon-like fluvial topography becomes smoother with increasing A_h. The profiles drawn in Fig. 4 confirm that the flanks of the valleys turn from almost vertical walls into straight hillslopes. The steepest segments of the profiles are as steep as expected according to Eq. (8) with A_h instead of A,

$$205 \quad S = \left(\frac{E}{K A_\mathrm{h}^m} \right)^{\frac{1}{n}} = A_\mathrm{h}^{-0.5}, \tag{14}$$

for $m = 0.5$, $n = 1$, $K = 1$, and $E = U = 1$. Less steep segments are an effect of the orientation of the hillslopes relative to the profile. For $A_\mathrm{h} = 1000$, the largest river is slightly lower than for the other topographies. However, this does not mean that it is less steep. We found that the channel slopes of all rivers satisfy the expected equilibrium relation (Eq. 8) except for some small deviations owing to the dynamic reorganization. The river is just slightly shorter.

210 Figure 5 shows the flow pattern of the region defined by the rectangle in Fig. 4c ($A_\mathrm{h} = 100$). About 60 % of the area belong to a small catchment with $A \approx 5000$. The smallest catchment size among the channels shown here is $A = 189 \approx 2A_\mathrm{h}$. In turn, the vast majority of the hillslope sites has a catchment size considerably below $A_\mathrm{h} = 100$. While the catchment size of hillslope sites has no immediate meaning in the model considered here, it is relevant for the effect of potential disturbances. If a hillslope site incises, its number of lower neighbors may decrease, so that it may turn into a channel site. If $A < A_\mathrm{h}$, however, its erosion
215 rate will decrease then, which counteracts incision. So it will likely be converted back into a hillslope site. In our numerical simulations, we found that practically all newly formed channel sites with $A < A_\mathrm{h}$ fall back to hillslope sites rapidly – often immediately in the next step.

However, there are also hillslope sites with $A > A_\mathrm{h}$. If such a site turns into a channel site, its erosion rate increases, which supports further incision. So hillslope sites with $A > A_\mathrm{h}$ may turn into stable channel sites. However, Fig. 5 reveals that planar
220 hillslopes with a parallel flow pattern are too short to reach the required catchment size. Hillslope sites with $A > A_\mathrm{h}$ are only
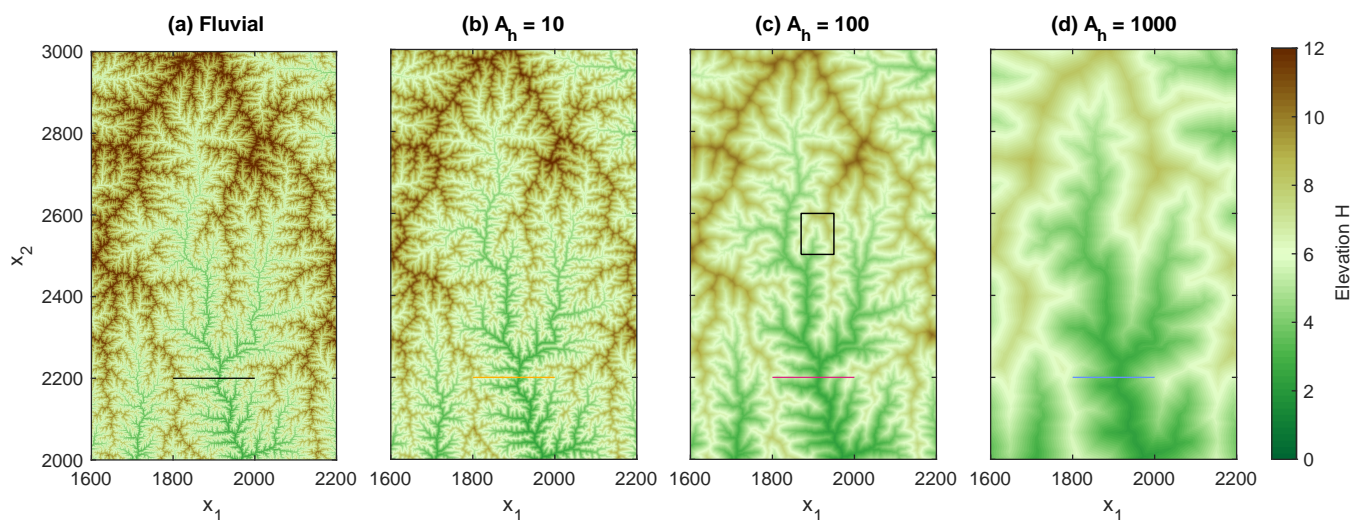
Figure 3. Part of the topography defined by the rectangle in Fig. 2 for different values of A_h. The profile lines refer to Fig. 4 and the rectangle to Fig. 5.
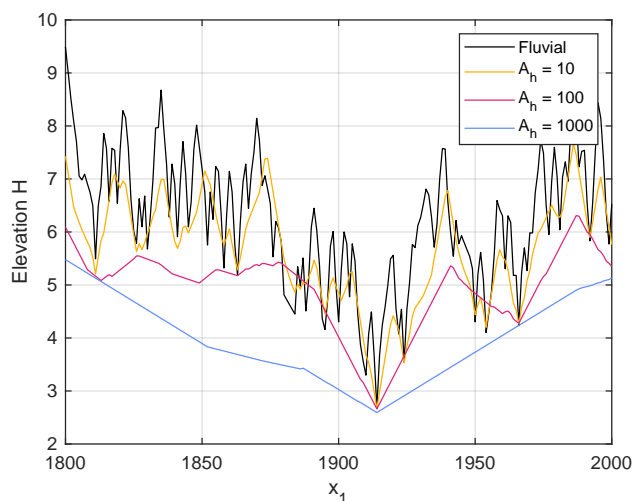
Figure 4. Topographic profiles along the lines defined in Fig. 3.

found where convergent flow occurs. These are predominantly regions above channel heads and above outer bends of existing channels.

The respective topography is shown in Fig. 6. Hillslopes with a parallel flow pattern in Fig. 5 correspond to planar, faceted areas. While the straight longitudinal profiles are directly related to the model used for hillslope erosion ($m = 0$), the occurrence
225 of planar patches is owing to the D8 scheme. As this scheme is not only used for computing the flow pattern (which is not
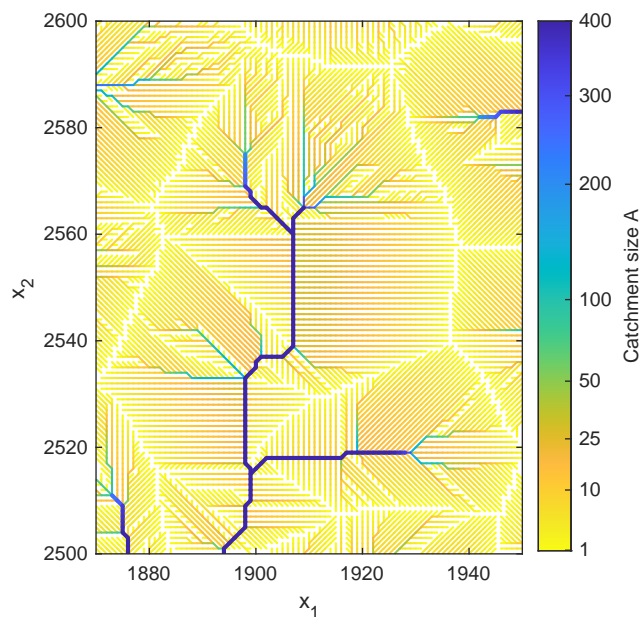
Figure 5. Drainage pattern of the the region defined by the rectangle in Fig. 4c. Channels are marked by thick lines. Hillslopes draining into straight river segments are typically characterized by a parallel flow pattern with catchment sizes considerably below $A_h = 100$. Catchment sizes $A \gtrless A_h$ occur preferably at convergent hillslopes above channel heads.
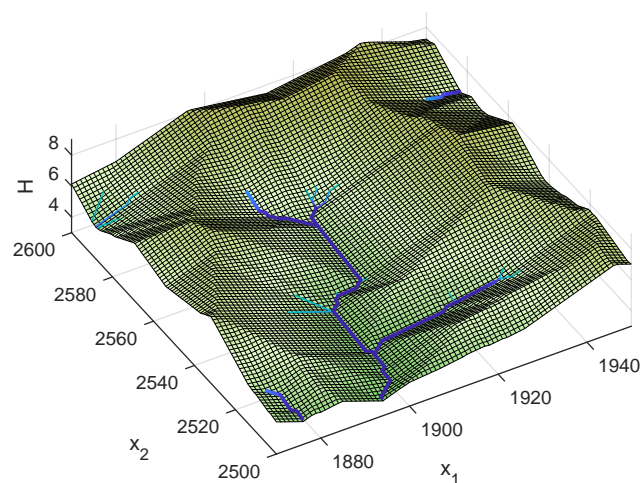
Figure 6. Topography of the domain shown in Fig. 5. Computing slope gradients based on the D8 scheme generates faceted, planar hillslopes.

immediately relevant at hillslopes), but also for computing the slope gradient, it enforces the formation of facets aligned either parallel to the coordinate axes or at a $45°$ angle.
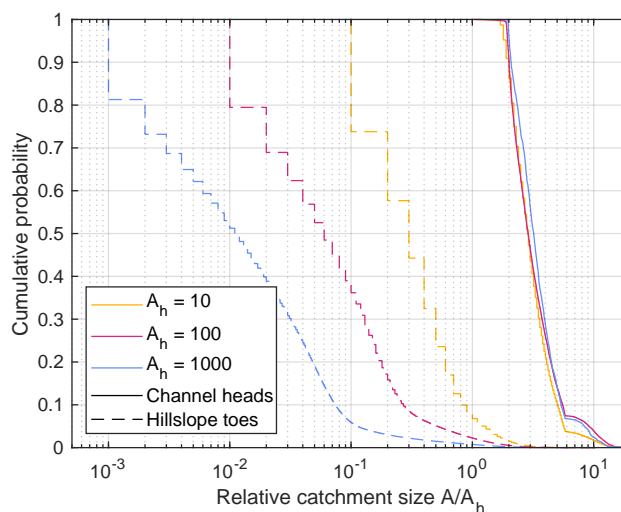
Figure 7. Empirical cumulative distributions of the catchment sizes of channel heads (solid lines) and hillslope toes (dashed lines).

A more detailed analysis of the catchment sizes over the entire domain is given in Fig. 7. The solid lines show the empirical cumulative distribution of the channel heads. The analysis is restricted to the channel heads instead of all channel sites for clarity
230 since the latter cover a much wider range of sizes. When rescaled to A_h, the channel heads follow very similar distributions for the considered values of A_h. In particular, the vast majority of all heads is in the range from $2A_h$ to $6A_h$. The similar distributions of the ratio $\frac{A}{A_h}$ show that A_h indeed controls the scale at which channels form, while it originally only defines the catchment size at which erosion in channels becomes stronger than on hillslopes. As a main result, however, we note that the channel initiation threshold is typically 2 to 6 times larger than A_h.

235 The dashed lines in Fig. 7 show the respective distribution for the hillslopes. Again for clarity, not all hillslope sites are analyzed, but only hillslope toes (hillslope sites that drain directly into a channel). It is immediately recognized that the catchment sizes at the hillslopes do not scale linearly with A_h. Owing to the dominance of parallel flow patterns at hillslopes, the catchment sizes at the toes rather scale linearly with the length of the hillslopes than with A_h. In our example, the different scaling of catchment sizes in channels and at hillslopes is not a problem since the catchment size is not relevant for the hill-
240 slopes. Otherwise, however, the results would be dependent on the spatial resolution, which should be avoided by referring to catchment size per unit width at hillslopes.

5 Scaling behavior

As discussed in Sect. 1, a dependence of the numerical results on the spatial resolution is an issue in many coupled models of fluvial erosion and hillslope processes. In order to find out whether the model considered here is free of such problems, we
245 need results obtained from simulations on lattices with different resolutions, but with the same model parameters. In principle, the simulations performed in the previous section on a grid with unit spacing can be rescaled accordingly.

Let us assign a value δx (in meters) to the unit grid spacing, a vertical length scale L to one nondimensional elevation unit, and a time scale T to one unit of nondimensional time. It is easily recognized from a dimensional analysis of Eq. (1) that the nondimensional erodibility K has to be rescaled by a factor

$$\alpha = \delta x^{n-2m} L^{1-n} T^{-1}. \tag{15}$$

Accordingly, the nondimensional uplift rate U must be rescaled by a factor $\beta = LT^{-1}$. So transferring the results of a nondimensional simulation with unit grid spacing to scenarios with a various values δx at constant K and U requires that α and β are constant, and thus

$$T \propto L \propto \delta x^{\frac{n-2m}{n}}. \tag{16}$$

For the combination $\frac{m}{n} = 0.5$ used here, this even implies that L and T are independent of δx. These results also hold for the the shared stream-power model (Eq. 3).

However, this scaling behavior is lost if a model for hillslope processes is included. For the model considered here, $\tilde{K}_{\mathrm{d}}$ and $\tilde{K}_{\mathrm{t}}$ scale differently from K_{d} and K_{t} (Eq. 15 with $m = 0$). This different scaling introduces a characteristic horizontal length scale. In terms of the parameter A_{h} defined in Eq. (13), this means that the real-world value of A_{h} scales with δx^2. In turn, keeping all erodibilities (and thus the real-world value of A_{h}) constant requires a scaling of the nondimensional value of A_{h} according to $A_{\mathrm{h}} \propto \delta x^{-2}$.

So our nondimensional simulations with $A_{\mathrm{h}} = 10$, 100, and 1000 can be interpreted as simulations with identical parameters, but different grid spacings δx and thus also different domain sizes. For comparing the results, the relief of all catchments is shown in Figure 8. The number of catchments ranges from 1237 for $A_{\mathrm{h}} = 1000$ to 157,339 for $A_{\mathrm{h}} = 10$. Since $A_{\mathrm{h}} \propto \delta x^{-2}$, the ratio $\frac{A}{A_{\mathrm{h}}}$ on the x-axis is proportional to the real-world catchment size.

Despite the scatter in the data, it is recognized that the relief increases logarithmically with the ratio $\frac{A}{A_{\mathrm{h}}}$ and that the data collapse quite well for different values of A_{h} as expected for $\frac{m}{n} = 0.5$. Fitting logarithmic functions confirms this finding. In particular, the functions obtained for $A_{\mathrm{h}} = 100$ and $A_{\mathrm{h}} = 1000$ are very close to each other and suggest the relation

$$\delta H = 2 \log_{10} \frac{A}{A_{\mathrm{h}}} + 1.75. \tag{17}$$

Although tested only for $\frac{m}{n} = 0.5$, these findings suggest that steady-state topographies are robust against the spatial resolution of the model. For time-dependent scenarios, however, the effect of the resolution should be investigated more thoroughly. The study on knickpoints by Hergarten (2021) would be a good starting point since major parts of the theory developed there could be adopted.

6 The break in slope

In the previous sections, we found that the concept for delineating channels developed in Sect. 2 works well in combination with a simple model for erosion at hillslopes and shows a reasonable scaling behavior. We now approach the question to what extent these results rely on the specific model and which parts can be generalized.
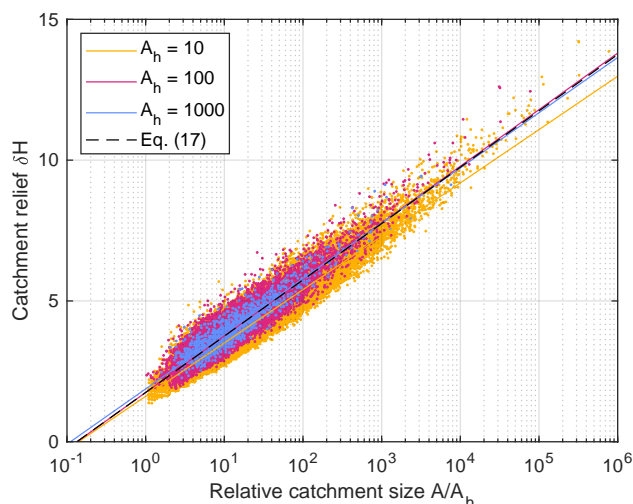
Figure 8. Relief of all catchments. The solid lines show fitted logarithmic functions, and the black dashed line corresponds to Eq. 17.
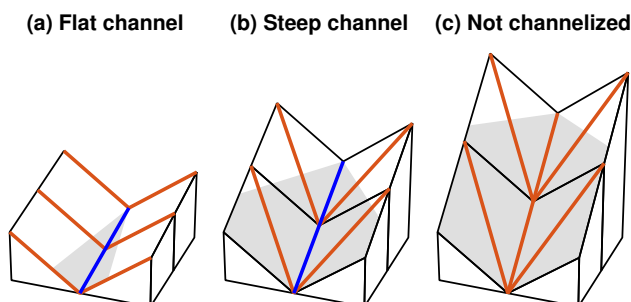
Figure 9. Three channel segments with different channel slopes. Blue lines refer to the flow directions of channelized flow. Red lines describe flow directions that do not satisfy the criterion for channelization. The area below the uppermost point of the channel is shaded.

As the most striking result, we found a shift in catchment sizes. While erosion in channels is stronger than at hillslopes for $A > A_\mathrm{h}$, almost all channel heads have catchment sizes $A > 2A_\mathrm{h}$. The following geometrical considerations show that this result is not specific to the considered model, but to the regular lattice with the D8 flow-routing scheme.

Three channel segments with different channel slopes are sketched in Fig. 9. If we apply the D8 scheme also to the hillslopes, the surrounding hillslopes are oriented perpendicular to the channel segment as long as the channel slope is quite low (Fig. 9a). For steeper channels, the D8 flow direction switches to the diagonal neighbor (Fig. 9b). Above a critical channel slope, sites in the valley have more than one lower neighbor, so that the channel no longer satisfies the criterion for channelization (Fig. 9c).

Figure 10 shows all possible scenarios for straight channel segments in plan view. For simplicity, unit grid spacing and unit slope at hillslopes are assumed. Let us start from an axis-parallel channel segment as illustrated in Fig. 10a, corresponding to Fig. 9. The elevations along the channel are $0, S, 2S, \ldots$, where S is the channel slope. If we apply the D8 scheme also to the hillslopes and assume that the channel is rather steep, the elevation of the red sites is $\sqrt{2}$ since they drain in diagonal direction
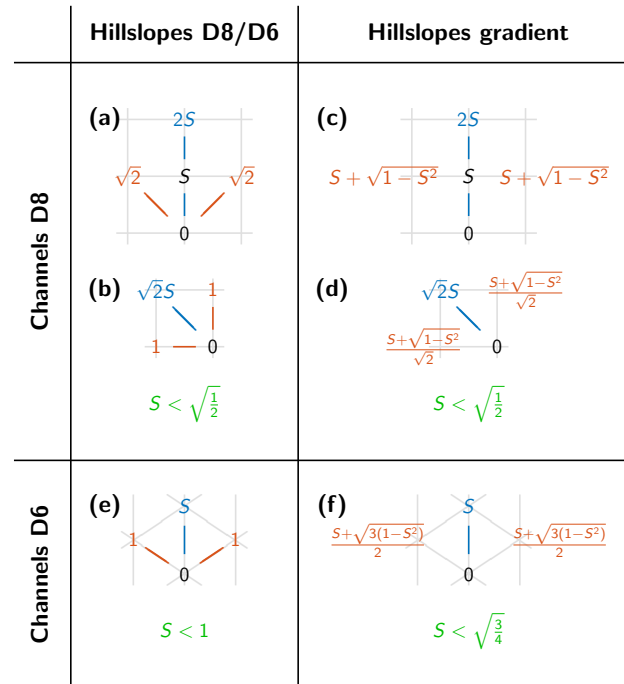
Figure 10. Geometry of channels and hillslopes for different topologies in plan view. Blue lines refer to flow in channels and red lines to flow on hillslopes if a single-flow-direction scheme is also used for hillslopes. Blue numbers are elevations of channel sites that must be lower than the elevations of the hillslope sites given by red numbers. Unit grid spacing is assumed, S is the channel slope, and the gradient of hillslopes is unity.

to a site with zero elevation. Then the blue site can only be channelized if its elevation is lower than those of the red sites, so

290   $2S < \sqrt{2}$.

For a diagonal channel segment (Fig. 10b), the elevation of the blue channel site must be $\sqrt{2}S$, while the elevation of the red hillslope sites is one due to their axis-parallel flow direction. So the condition for the channelization of the blue site is $\sqrt{2}S < 1$.

In both cases, the condition for channelization is $S < \sqrt{\frac{1}{2}}$. So slopes in channels must be at least by a factor of $\sqrt{\frac{1}{2}}$ lower

295   than at the surrounding hillslopes. In order to achieve the same erosion rate, the catchment size must be

$$A = \sqrt{2}^{\frac{n}{m}} A_{\mathrm{h}} = 2^{\frac{1}{2\theta}} A_{\mathrm{h}} = 2A_{\mathrm{h}} \tag{18}$$

for $\theta = 0.5$ in the channel according to Eqs. (8) and (14). So the finding $A > 2A_{\mathrm{h}}$ relies on the D8 scheme and on our choice $\theta = 0.5$.

The break in slope by a factor of $\sqrt{\frac{1}{2}}$ for all orientations (axis-parallel or diagonal) of the channel segment is crucial for

300   the applicability of the D8 scheme. If the factors were different, we would expect problems with anisotropy. Then either

axis-parallel or diagonal channel segments would be preferred in the upper ranges of rivers in combination with a preferred orientation of the surrounding hillslopes.

Using a representation of the gradient by difference quotients at hillslopes does even not affect the factor $\sqrt{\frac{1}{2}}$ (Fig. 10c,d). In order to obtain a total slope of one at a given channel slope S, the slope perpendicular to the channel must be $\sqrt{1 - S^2}$.

305 This yields an elevation of $S + \sqrt{1 - S^2}$ for the red site in Fig. 10c. For a diagonal channel segment (Fig. 10d), the respective elevation is by a factor of $\sqrt{\frac{1}{2}}$ lower due to the shorter distances. In both cases, the obtained criterion for channelization is $S < \sqrt{\frac{1}{2}}$ and thus the same as before. So it makes no difference for the break in slope between hillslopes and channels whether we allow arbitrary slope directions at hillslopes or use the D8 scheme.

The $45°$ steps in flow direction are the reason why the simple D8 scheme performs well in combination with the criterion

310 for channel formation. Hillslopes are perpendicular to large channels (small channel slope) and are aligned at a $45°$ angle for the steepest possible channels. So the D8 scheme captures both end-members well. Only hillslope sites that drain directly into a diagonal channel segment are an exception since the D8 scheme only allows a $45°$ angle here. However, this is not a serious issue since it only concerns a single row of sites and does not affect the rest of the hillslopes.

Orientations between these two end-members are not captured if the simple D8 scheme is applied to the hillslopes. However,

315 we did not encounter any obvious artifacts that could be related to this limitation. So the simple D8 scheme appears to be well-suited not only for the channels, but also for the hillslopes. This is an advantage for the numerical implementation since it allows for a seamless application of the fully implicit scheme proposed by Hergarten (2020b).

An isometric grid consisting of equilateral triangles may provide a better isotropy than a regular grid at first sight. If the gradient is used for the hillslopes, the slope break between hillslopes and channels is smaller than for the D8 scheme, owing

320 to the lower number of competing neighbors (6 instead of 8). As illustrated in Fig. 10f, the respective factor is $\sqrt{\frac{3}{4}}$ instead of $\sqrt{\frac{1}{2}}$. More important, the slope break vanishes completely if we use the slope towards the lowest neighbor (called D6 in Fig. 10) at hillslopes (Fig. 10e). Furthermore, the restriction to the lowest neighbor aligns all hillslopes at an angle of $60°$ towards the respective channels, so that the gradient of hillslopes draining into large channels (with low channel slopes) would not be captured well. While we did not perform any numerical tests on triangular grids, these results suggest that regular grids

325 in combination with the D8 scheme are better in this context, owing to the $45°$ steps in direction.

7 Defining channel thresholds explicitly

In its spirit, the idea of distinguishing channels from hillslopes by the topography differs from the established concept, which assumes a threshold catchment size A_c for channelization. As a major difference, the topography-based approach does not enforce a strict threshold for the initiation of channels. For the model investigated in Sect. 4, most of the channel heads are

330 in the range $2A_h \leq A \leq 6A_h$. Beyond this variation by a factor of three, A_h depends on the parameters of the erosion models since it was defined as the catchment size at which channel erosion becomes more efficient than hillslope erosion.

In order to find out to what extent both approaches differ practically, we performed simulations with the same model, but with an explicit threshold A_c for channelization instead of the criterion based on the number of lower neighbors. Figure 11
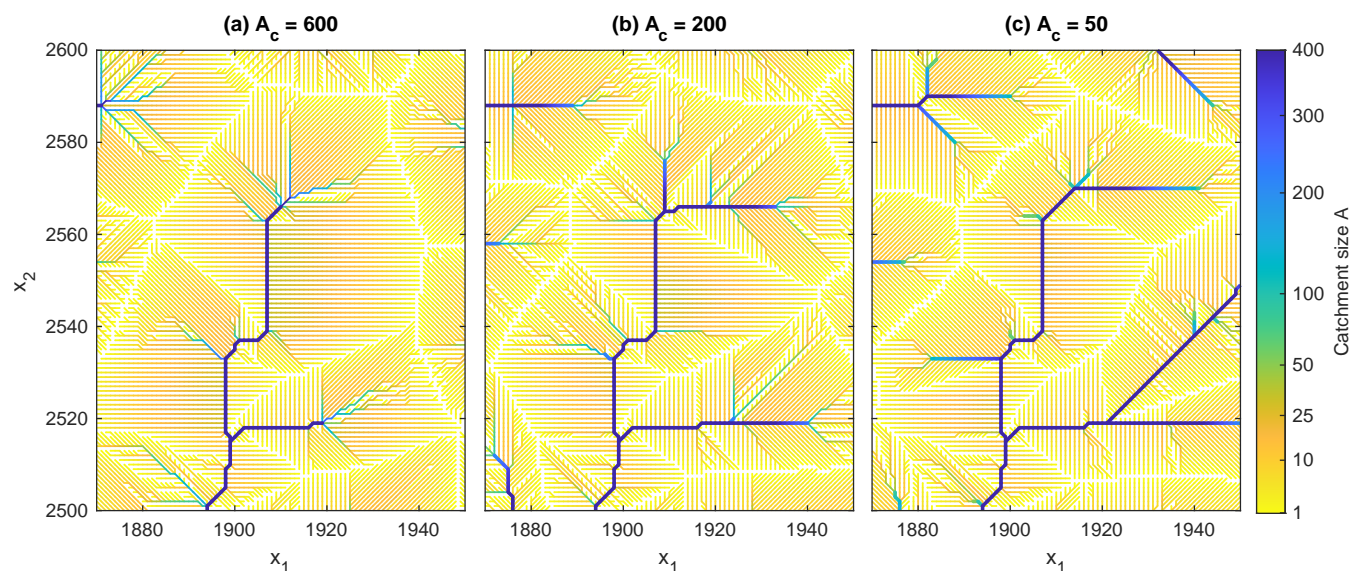
Figure 11. Drainage pattern of the the region shown in Fig. 5 for $A_\mathrm{h} = 100$ and different values of the channelization threshold A_c. Channels are marked by thick lines.

shows the drainage pattern of the region from Fig. 5 for different values of A_c. All model parameters are the same as in Sect. 4,

335 including $A_\mathrm{h} = 100$. The threshold value $A_\mathrm{c} = 600$ (Fig. 11a) then corresponds to the maximum catchment size of more than 90 % of all channel heads in the self-organizing model (Fig. 7). In turn, $A_\mathrm{c} = 200$ (Fig. 11b) corresponds to the minimum catchment size obeyed by almost all channel sites in the self-organizing model. For $A_\mathrm{c} = 50$ (Fig. 11c), channel segments may be steeper than the surrounding hillslopes, which makes channels with $A < 100$ unstable.

The pattern of the largest rivers (which are still rather small) is identical to that from Fig. 5. Measured over the entire

340 topography, only about 3 to 5 % of all sites with $A \geq 1000$ change their flow direction compared to the model without threshold. As expected, the channels extend more into the hillslopes with decreasing A_c. As a consequence, the upper parts of the channels tend to be unstable, which leads to an increased frequency of reorganization.

This effect is immediately recognized in the analysis of the channel slopes shown in Fig. 12. While the equilibrium channel slope is $S = A^{-0.5}$ according to Eq. (8), a considerable scatter is found in the actual channel slopes. This scatter decreases

345 with increasing A_c, but is stronger than for the topography-based criterion for all considered values of A_c. Accordingly, there is a strong variation in erosion rates, which indicates a rapid reorganization of the drainage pattern at small catchment sizes. The resulting fluctuations in sediment flux are responsible for the downstream propagation of the scatter, which is still visible at $A = 10000$.

A distinct change in channel slopes occurs at $A = A_\mathrm{h}$ (which requires $A_\mathrm{c} < A_\mathrm{h}$). The systematic decrease in S with A is

350 even lost for $A < A_\mathrm{h}$. This is the situation where equilibrium channels would be steeper than hillslopes and thus cannot be stable. Then the headwaters are formally channels ($A > A_\mathrm{c}$), but rather hillslopes in their properties. So the erosion law (the
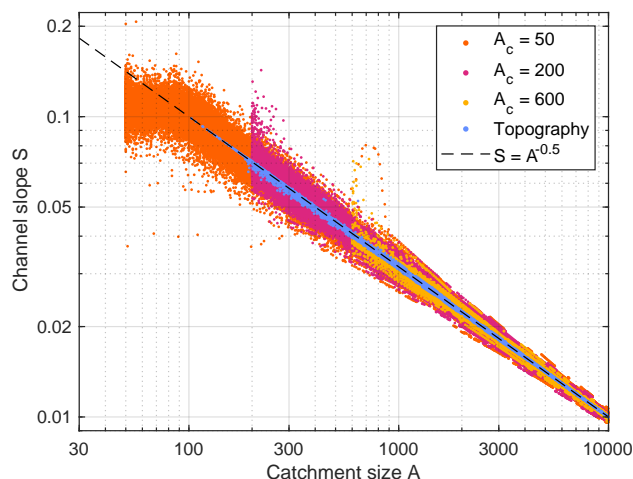
Figure 12. Channel slopes of all channelized sites for $A_h = 100$ and different values of the channelization threshold A_c. The blue dots refer to the topography-based criterion without threshold. The dashed line shows the theoretical equilibrium relation $S = A^{-0.5}$ (Eq. 8).

efficiency of hillslope erosion compared to fluvial erosion, expressed by A_h here) overrides the threshold of channelization in this case.

These results suggest that the model somehow counteracts the imposed threshold A_c by permanently switching between
355   channels and hillslopes for all considered values of $A = A_c$. It looks as if this model was constrained too strongly. In each case, using different models for channels and hillslopes introduces a characteristic catchment size A_h above which channels erode more efficiently than hillslopes. Defining a second characteristic catchment size by imposing a threshold at which hillslopes turn into channels seems to be a condition too many.

While the formation of temporary channels on hillslopes is not necessarily unrealistic, it may also make the model more
360   complicated from a theoretical point of view. Since catchment size is not well-defined on hillslopes, it may generate artifacts. However, analyzing the relief the same way as in Fig. 8 did not reveal any obvious scaling issues. So we cannot pinpoint any clear problem of the concept based on a threshold catchment size for the transition to channelized flow at this stage.

8   Conclusions

In this study, a new concept for coupling fluvial erosion and sediment transport with hillslope processes in landform evolution
365   models is proposed. In contrast to the widely used approach based on a threshold catchment size for channelized flow, this concept directly uses the topography. Channelized flow is assumed for all sites of a discrete grid that have only one neighbor with a lower elevation. This definition reflects the idea that a thin layer of water is focused into a single direction without spreading laterally.

In order to test the concept numerically, we combined the shared stream-power model for fluvial erosion with a simple model
370   for hillslopes, where the erosion rate only depends on slope. As a main result, the topography self-organizes into channels and

hillslopes. Channel heads form in a certain range of catchment sizes. This range depends on the catchment size at which erosion in channels is more efficient than at hillslopes (A_h in the formulation used here), but is considerably higher. So the actual transition from hillslopes to channels takes place at larger catchment sizes where erosion in channels is substantially more efficient than at hillslopes. This effect can be explained by a gap in slopes between channels and hillslopes. For the simple

375   D8 flow-routing scheme, channels must be at least by a factor of $\sqrt{\frac{1}{2}}$ less steep than hillslopes.

The numerical tests revealed no obvious dependence of the results on the spatial resolution, which is a problem in some other coupled models of fluvial erosion and hillslope processes. The approach works well even if the D8 scheme is used for computing gradients at hillslopes. While this simplification allows for a seamless coupling of fluvial erosion and hillslope processes, it enforces the formation of faceted areas on hillslopes in combination with a permanent reorganization. However,

380   the effects of this reorganization on the large-scale topography seem to be minor.

Finally, the question arises whether the topography-based delineation of channels proposed here is better than defining a threshold catchment size explicitly. Our numerical tests revealed that the coupled model apparently counteracts the imposition of a threshold by a strong reorganization, which also affects the channel slopes of the rivers. However, we did not encounter any serious problems arising from this behavior. So the topography-based delineation of channels is more elegant than imposing a

385   threshold and leads to a nicer behavior of the model, but this does not mean that it captures the real-world behavior better. In this context, the question is whether stream-power models of fluvial erosion become invalid if the flow is not sufficiently confined to a single channel or rather if the discharge is too low. Addressing this question requires further research. Nevertheless, the delineation of channels by topography provides a simple concept for coupling fluvial erosion with hillslope processes that works quite well.

390   *Code and data availability.* All codes are available in a Zenodo repository at https://doi.org/10.5281/zenodo.6794117 (Hergarten, 2022c). This repository also contains the data obtained from the numerical simulations. Users who are interested in using the landform evolution model OpenLEM in their own research are advised to download the most recent version from http://hergarten.at/openlem (Hergarten, 2022b). The authors are happy to assist interested readers in reproducing the results and performing subsequent research.

Author contributions. S.H. developed the theoretical framework and the numerical codes. Both authors wrote the paper.

395   *Competing interests.* The authors declare that there is no conflict of interest.

Acknowledgements. This work was funded by the Deutsche Forschungsgemeinschaft (DFG, German Research Foundation) – 432703650.

References

Adams, B. A., Whipple, K. X., Forte, A. M., Heimsath, M., and Hodges, K. V.: Climate controls on erosion in tectonically active landscapes, Sci. Adv., 6, eaaz3166, https://doi.org/10.1126/sciadv.aaz3166, 2020.

400 Bonetti, S., Bragg, A., and Porporato, A.: On the theory of drainage area for regular and non-regular points, Proc. R. Soc. Lond., 474, 20170 693, https://doi.org/10.1098/rspa.2017.0693, 2018.

Braun, J. and Willett, S. D.: A very efficient O(n), implicit and parallel method to solve the stream power equation governing fluvial incision and landscape evolution, Geomorphology, 180–181, 170–179, https://doi.org/10.1016/j.geomorph.2012.10.008, 2013.

Campforts, B., Schwanghart, W., and Govers, G.: Accurate simulation of transient landscape evolution by eliminating numerical diffusion:
405 the TTLEM 1.0 model, Earth Surf. Dynam., 5, 47–66, https://doi.org/10.5194/esurf-5-47-2017, 2017.

Carretier, S., Martinod, P., Reich, M., and Godderis, Y.: Modelling sediment clasts transport during landscape evolution, Earth Surf. Dynam., 4, 237–251, https://doi.org/10.5194/esurf-4-237-2016, 2016.

CNIG: Centro de Descargas, http://centrodedescargas.cnig.es, last access: 09.04.2022, 2022.

Coulthard, T. J.: Landscape evolution models: a software review, Hydrol. Process., 15, 165–173, https://doi.org/10.1002/hyp.426, 2001.

410 Davy, P. and Lague, D.: Fluvial erosion/transport equation of landscape evolution models revisited, J. Geophys. Res. Earth Surf., 114, F03 007, https://doi.org/10.1029/2008JF001146, 2009.

Freeman, G. T.: Calculating catchment area with divergent flow based on a rectangular grid, Comp. Geosci., 17, 413–422, https://doi.org/10.1016/0098-3004(91)90048-I, 1991.

Hack, J. T.: Studies of longitudinal profiles in Virginia and Maryland, no. 294-B in US Geol. Survey Prof. Papers, US Government Printing
415 Office, Washington D.C., https://doi.org/10.3133/pp294B, 1957.

Harel, M.-A., Mudd, S. M., and Attal, M.: Global analysis of the stream power law parameters based on worldwide [10]Be denudation rates, Geomorphology, 268, 184–196, https://doi.org/10.1016/j.geomorph.2016.05.035, 2016.

Hergarten, S.: Rivers as linear elements in landform evolution models, Earth Surf. Dynam., 8, 367–377, https://doi.org/10.5194/esurf-8-367-2020, 2020a.

420 Hergarten, S.: Transport-limited fluvial erosion – simple formulation and efficient numerical treatment, Earth Surf. Dynam., 8, 841–854, https://doi.org/10.5194/esurf-8-841-2020, 2020b.

Hergarten, S.: The influence of sediment transport on stationary and mobile knickpoints in river profiles, J. Geophys. Res. Earth Surf., 126, e2021JF006 218, https://doi.org/10.1029/2021JF006218, 2021.

Hergarten, S.: Theoretical and numerical considerations of rivers in a tectonically inactive foreland, Earth Surf. Dynam., 10, 671–686,
425 https://doi.org/10.5194/esurf-10-672-2022, 2022a.

Hergarten, S.: OpenLEM, http://hergarten.at/openlem, last access: 04.07.2022, 2022b.

Hergarten, S.: Self-organization of channels and hillslopes, https://doi.org/10.5281/zenodo.6794117, 2022c.

Hergarten, S. and Neugebauer, H. J.: Self-organized critical drainage networks, Phys. Rev. Lett., 86, 2689–2692, https://doi.org/10.1103/PhysRevLett.86.2689, 2001.

430 Hilley, G. E., Porder, S., Aron, F., Baden, C. W., Johnstone, S. A., Liu, F., Sare, R., Steelquist, A., and Young, H. H.: Earth's topographic relief potentially limited by an upper bound on channel steepness, Nature Geosci., 12, 828–832, https://doi.org/10.1038/s41561-019-0442-3, 2019.

Howard, A. D.: Theoretical model of optimal drainage networks, Water Resour. Res., 26, 2107–2117, https://doi.org/10.1029/WR026i009p02107, 1990.

435 Howard, A. D.: A detachment-limited model for drainage basin evolution, Water Resour. Res., 30, 2261–2285, https://doi.org/10.1029/94WR00757, 1994.

Lague, D.: The stream power river incision model: evidence, theory and beyond, Earth Surf. Process. Landforms, 39, 38–61, https://doi.org/10.1002/esp.3462, 2014.

O'Callaghan, J. F. and Mark, D. M.: The extraction of drainage networks from digital elevation data, Computer Vision, Graphics, and Image 440 Processing, 28, 323–344, https://doi.org/10.1016/S0734-189X(84)80011-0, 1984.

Pelletier, J. D.: Minimizing the grid-resolution dependence of flow-routing algorithms for geomorphic applications, Geomorphology, 122, 91–98, https://doi.org/10.1016/j.geomorph.2010.06.001, 2010.

Perron, J. T.: Numerical methods for nonlinear hillslope transport laws, J. Geophys. Res. Earth Surf., 116, F02 021, https://doi.org/10.1029/2010JF001801, 2011.

445 Perron, J. T., Dietrich, W. E., and Kirchner, J. W.: Controls on the spacing of first-order valleys, J. Geophys. Res. Earth Surf., 113, F04 016, https://doi.org/10.1029/2007JF000977, 2008.

Quinn, P. F., Beven, K. J., Chevallier, P., and Planchon, O.: The prediction of hillslope flow paths for distributed hydrological modeling using digital terrain models, Hydrol. Process., 5, 59–79, https://doi.org/10.1002/hyp.3360050106, 1991.

Rinaldo, A., Rodriguez-Iturbe, I., Bras, R. L., Ijjasz-Vasquez, E., and Marani, A.: Minimum energy and fractal structures of drainage net- 450 works, Water Resour. Res., 28, 2181–2195, https://doi.org/10.1029/92WR00801, 1992.

Rinaldo, A., Rodriguez-Iturbe, I., and Rigon, R.: Channel networks, Annu. Rev. Earth Planet. Sci., 26, 289–327, https://doi.org/10.1146/annurev.earth.26.1.289, 1998.

Rodriguez-Iturbe, I., Rinaldo, A., Rigon, R., Bras, R. L., Ijjasz-Vasquez, E., and Marani, A.: Fractal structures as least energy patterns: The case of river networks, Geophys. Res. Lett., 19, 889–892, https://doi.org/10.1029/92GL00938, 1992a.

455 Rodriguez-Iturbe, I., Rinaldo, A., Rigon, R., Bras, R. L., Marani, A., and Ijjasz-Vasquez, E.: Energy dissipation, runoff production, and the three-dimensional structure of river basins, Water Resour. Res., 28, 1095–1103, https://doi.org/10.1029/91WR03034, 1992b.

Roering, J. J., Kirchner, J. W., and Dietrich, W. E.: Evidence for nonlinear, diffusive sediment transport on hillslopes and implications for landscape morphology, Water Resour. Res., 35, 853–870, https://doi.org/10.1029/1998WR900090, 1999.

Tarboton, D. G.: A new method for the determination of flow directions and upslope areas in grid Digital Elevation Models, Water Resour. 460 Res., 33, 309–319, https://doi.org/10.1029/96WR03137, 1997.

van der Beek, P.: Modelling landscape evolution, in: Environmental Modelling: Finding Simplicity in Complexity, edited by Wainwright, J. and Mulligan, M., pp. 309–331, Wiley-Blackwell, Chichester, 2 edn., 2013.

Whipple, K. X. and Tucker, G. E.: Implications of sediment-flux-dependent river incision models for landscape evolution, J. Geophys. Res., 107, 2039, https://doi.org/10.1029/2000JB000044, 2002.

465 Whipple, K. X., DiBiase, R. A., and Crosby, B. T.: Bedrock rivers, in: Fluvial Geomorphology, edited by Shroder, J. and Wohl, E., vol. 9 of *Treatise on Geomorphology*, pp. 550–573, Academic Press, San Diego, CA, https://doi.org/10.1016/B978-0-12-374739-6.00254-2, 2013.

Willgoose, G.: Mathematical modeling of whole landscape evolution, Annu. Rev. Earth Planet. Sci., 33, 443–459, https://doi.org/10.1146/annurev.earth.33.092203.122610, 2005.

Wobus, C., Whipple, K. X., Kirby, E., Snyder, N., Johnson, J., Spyropolou, K., Crosby, B., and Sheehan, D.: Tectonics from topogra- 470 phy: Procedures, promise, and pitfalls, in: Tectonics, Climate, and Landscape Evolution, edited by Willett, S. D., Hovius, N., Bran-

don, M. T., and Fisher, D. M., vol. 398 of *GSA Special Papers*, pp. 55–74, Geological Society of America, Boulder, Washington, D.C., https://doi.org/10.1130/2006.2398(04), 2006.

Yuan, X. P., Braun, J., Guerit, L., Rouby, D., and Cordonnier, G.: A new efficient method to solve the stream power law model taking into account sediment deposition, J. Geophys. Res. Earth Surf., 124, 1346–1365, https://doi.org/10.1029/2018JF004867, 2019.